



This is a repository copy of *Hardness characterisation of grey cast iron and its tribological performance in a contact lubricated with soybean oil.*

White Rose Research Online URL for this paper:  
<http://eprints.whiterose.ac.uk/105870/>

Version: Accepted Version

---

**Article:**

Bahari, A., Lewis, R. and Slatter, T. [orcid.org/0000-0002-0485-4615](https://orcid.org/0000-0002-0485-4615) (2018) Hardness characterisation of grey cast iron and its tribological performance in a contact lubricated with soybean oil. *Proceedings of the Institution of Mechanical Engineers, Part C: Journal of Mechanical Engineering Science*, 232 (1). pp. 190-203. ISSN 0954-4062

<https://doi.org/10.1177/0954406216675895>

---

Bahari A, Lewis R, Slatter T. Hardness characterisation of grey cast iron and its tribological performance in a contact lubricated with soybean oil. *Proceedings of the Institution of Mechanical Engineers, Part C: Journal of Mechanical Engineering Science*. 2018;232(1):190-203. Copyright © 2016 IMechE. DOI: 10.1177/0954406216675895. Article available under the terms of the CC-BY-NC-ND licence (<https://creativecommons.org/licenses/by-nc-nd/4.0/>).

**Reuse**

This article is distributed under the terms of the Creative Commons Attribution-NonCommercial-NoDerivs (CC BY-NC-ND) licence. This licence only allows you to download this work and share it with others as long as you credit the authors, but you can't change the article in any way or use it commercially. More information and the full terms of the licence here: <https://creativecommons.org/licenses/>

**Takedown**

If you consider content in White Rose Research Online to be in breach of UK law, please notify us by emailing [eprints@whiterose.ac.uk](mailto:eprints@whiterose.ac.uk) including the URL of the record and the reason for the withdrawal request.



[eprints@whiterose.ac.uk](mailto:eprints@whiterose.ac.uk)  
<https://eprints.whiterose.ac.uk/>

# **Hardness characterisation of grey cast iron and its tribological performance in a contact lubricated with soybean oil**

**\*Adli Bahari, Roger Lewis, Tom Slatter**

Department of Mechanical Engineering, University of Sheffield, Mappin Street, United Kingdom, S1 3JD

\*Corresponding author: E-mail address: [adlibhr@gmail.com](mailto:adlibhr@gmail.com) (Adli Bahari)

## **Abstract**

The effect of hardness of grey cast iron flat specimen on its wear and friction on the contact were characterised with the presence of vegetable oil as biolubricant. Prior to the tribological test, the as-received grey cast iron flat specimen hardness was characterised. Friction and wear tests were then conducted using a ball-on-flat reciprocating sliding contact. The one-way analysis of variance (ANOVA) was used to determine the significance of friction and wear data with a 95% significance level. The wear scars after the test were then characterised by surface roughness and wear mechanism. The microstructure and elemental analysis were also reported. The average value of hardness was 210 HV with a large difference between minimum (185 HV) and maximum (250 HV) values. The friction and wear performance of grey cast iron specimens with soybean oil varied with its hardness. The specimens with higher hardness gave lower friction coefficient and greater wear resistance than the lower hardness specimens. The difference in coefficient of friction produced between high hardness specimens (COF = 0.122) and low hardness specimens (COF = 0.140) was 17%. In terms of mass loss, the low hardness

specimens (mass loss = 50.38 mg) and the high hardness specimens (mass loss = 12.90 mg) produced a difference of 74%. It is shown that, with soybean oil lubricant, the grey cast iron specimen can produce wide range of tribological data especially on mass loss due to its hardness distribution. The influence of soybean oil lubrication in this work is less in improving the wear resistance (about 7%), but greater for friction reduction (about 24%) compared to an unlubricated grey cast iron surface. The hardness of grey cast iron specimen is an important parameter that needs to be specifically measured and controlled on the contact due to wide hardness distribution of grey cast iron may produce variation in tribological data.

**Keywords:** hardness, grey cast iron, biolubricants, wear

## **INTRODUCTION**

Grey cast iron (GCI) has been known for its good tribological properties such as low friction and high wear resistance, for example it is a common material for the piston ring and cylinder liner contact in internal combustion engines <sup>1</sup>. Typically comprising iron, silicon, manganese, sulphur, phosphorus and 2.5 to 4.0% carbon <sup>2</sup> in the form of flake graphite, it provides a solid lubrication film, that gives excellent wear and friction characteristics under a dry sliding contact <sup>3</sup>. The effects of metal hardness on tribological performance in dry, or lubricated, contacts are well reported <sup>4-6</sup>. It was shown that in a dry contact, pure materials with high hardness gave lower friction than softer materials <sup>7</sup>. The high hardness is attributed to the presence of stronger atomic bonds increasing the resistance to adhesion <sup>7</sup>. Furthermore, the low hardness material allowed more indentation to the surface thus increasing the track width and

ploughing force <sup>8</sup>. However, in a lubricated contact, the friction coefficient for heat treated carbon steel was independent of specimen hardness, while in dry contact, friction was lower for harder material <sup>9</sup>.

In conducting tribological tests related to GCI, specimen hardness is one of the vital mechanical properties that needs to be evaluated prior to testing. The variation of reported hardness, even in 'standard' GCI is high. The difference between maximum and minimum hardness value of GCI grades designated within EN 1561 is 60 HB <sup>10</sup>. Shturmakov <sup>11</sup> also found that GCI ASTM 35B (equivalent to EN 1561 EN-GJL 250) produced the same range (59.4 HB). Others presented the hardness value for this material in various ranges, such as 220-240HV and 207-255 HB <sup>12, 13</sup>. However, there are a few reports ignoring this range and using bulk value of GCI hardness as a single value (265 HV <sup>3</sup> and 195 HB <sup>14</sup>) of hardness to further conducting their tribological test.

The effect of cast iron specimen hardness on friction and wear has been reported <sup>15</sup> mainly under dry sliding contact condition but the specimen hardness is presented as specific bulk value and the nature of the hardness measurement is not mentioned. Sugishita <sup>15</sup> performed friction tests (pin-on-disc) on different heat treated spheroidal graphite cast irons (hardness range 300 ~ 1000 HV) and found the friction coefficient (0.11 ~ 0.21) was inversely proportional with material hardness in the solid lubrication condition when the hardness was less than 400 HV. However, when the hardness was more than 400 HV, the friction coefficient was proportional to material hardness <sup>15</sup>. In order to produce robust tribological data (friction and wear), the hardness tests need to be carried out on the sliding surface as commercially available GCI presents a wide range of hardness values <sup>11</sup>. This wide range is typically attributed to the heterogeneous microstructure <sup>2</sup> and the uneven size and distribution of flake graphite <sup>16</sup> caused by the different

cooling rate of material during the solidification process in the mould tool <sup>17</sup>. Hence, the bulk value of specimen hardness may differ from the value in the wear scar area. This could lead to misrepresentation of the GCI tribological data-hardness relation to be analysed.

The lubrication effects of vegetable derived oils on cast irons have been studied, but the works are limited to palm oil and jatropha oil and the hardness of the specimens is not specified <sup>18, 19</sup>. The tribological performance of soybean oil and its chemically modified oils also have been reported, but the tests mainly using a four ball tribometer <sup>20-22</sup> which is based on a rotating steel ball pressed against three fixed steel balls. The hardness effects of GCI on friction and wear would be an interesting subject if it is further studied with vegetable oil (soybean oil) as a biolubricant under reciprocating sliding contact with rigorous hardness characterisation of the counterface. Interest in biolubricant research is increasing because of its potential as an alternative lubricant to mineral oil. Biolubricants are renewable base stocks, biodegradable, less-toxic and environmentally friendly <sup>23</sup>. When compared to mineral oil, biolubricant have higher viscosity index, higher flash point and better in lubricity <sup>24</sup>.

In this work, the hardness test of GCI specimen was carried out specifically on the intended wear scar region prior to test. The response of friction and wear over a range of specimen hardnesses with a soybean oil lubricated contact were examined. To support the main result, the surface morphology and elemental analysis are presented.

## **EXPERIMENTAL**

### **Specimens and Lubricant**

A ball on flat reciprocating sliding contact was used to evaluate the wear and friction behaviour of GCI on soybean oil lubricated surface. The flat rectangular specimen (66 mm x 25 mm x 4 mm) was GCI (EN1561-GJL-250). The surface finishing of the flat specimen was ground to an average surface roughness,  $R_a = 0.15 \mu\text{m}$ . The ball specimen (6 mm diameter) is made of chrome steel AISI 52100 with average surface roughness,  $R_a = 0.03 \mu\text{m}$ , and held firmly by a brass tube. The geometry of both specimens is depicted in Fig. 1.

A commercial soybean oil (Clearspring) was used as the lubricant because soybean oil is one of the most common vegetable oils globally. This oil is an organic type which made using a cold pressed process without additional chemicals to maintain its purity. The main physical properties of the soybean oil are listed in Table 1.

### **Hardness Test**

A microhardness test was used in order to minimise the indentation size on the specimens. A Vickers hardness tester with 20 kg applied load was used on the GCI flat specimens to measure the hardness of the intended wear scar area (Scar 1, Scar 2 and Scar 3) as shown in Fig. 2. The average hardness based on these three points then was calculated to characterise the hardness of each wear scar area before testing. A number of 426 intended wear scars were used to perform the hardness measurements which represent 426 specimens. In order

to facilitate the test and analysis, 9 specimens were then selected and divided into 3 groups (low, medium and high hardness) based on their hardness value. The friction and wear test was then conducted on these 9 specimens.

### **Friction and Wear Test**

Selected specimens, as discussed in Section 2.1, were then tested. A Phoenix Tribology/Plint TE77 test rig (Fig. 3) was used for measuring the coefficient of friction (COF) by means of a calibrated load cell. The linear reciprocating motion on the test rig could resemble the motion of a piston ring in an internal combustion engine. The tests were run at a temperature of  $100 \pm 2$  °C, to replicate the oil temperature in the sump of an internal combustion engine<sup>25</sup>. A mean sliding speed of  $0.13 \pm 0.01$  m/s and a stroke length of  $15 \pm 0.1$  mm was selected and the test duration was 1 hr. A point contact (ball on flat) was chosen in order to eliminate the misalignment problem on counterface of contact bodies. All parameters were selected based on preliminary experiments conducted to ensure the production of measureable wear scars. Thus, a normal load 40 N applied to the ball was selected based on trial and error. Specimen masses were measured before and after the test and the difference recorded as the mass loss of the specimen. Single variable ANOVA statistical analysis (level of confidence 95%) was performed to recognise the significant of friction and wear data. In this analysis, the null hypothesis is defined as: “all means of experimental data are equal”. The probability of obtaining this null hypothesis is defined as P in which lower P value is an indication of strong evidence to reject the null hypothesis. In this study, data points are statistically significant if the significance level, P value < 0.05.

The minimum lubricant film thickness,  $h_{\min}$  was calculated using the formula given by Hamrock et al.<sup>26</sup>. The lubrication regime is determined based on the lambda value ( $\lambda = h_{\min}/\sigma^*$ ) given by Hutchings<sup>27</sup> where  $\sigma^*$  is the root mean square roughness of the two contacting surfaces.

### **Surface Topography, Morphology and Elemental Analysis**

The GCI flat specimens were removed from the test rig after 60 min and were cleaned in acetone and rinsed in isopropanol for 5 min each using an ultrasonic cleaner. The surface roughness measurements were conducted across the wear scar at several points and waviness at the centre line and along the wear scar. A reflected light optical microscope was used to obtain images of the worn surfaces in order to identify the wear in a broader view. Scanning electron microscopy (SEM) was used to inspect the worn specimens at a much higher magnification than the optical microscope in order to investigate the wear mechanisms. The electron dispersive analysis of X-rays (EDX) was coupled with the SEM in order to analyse the elements that exist on the worn surfaces.

## **RESULTS AND DISCUSSION**

### **Hardness Properties**

The distributions of wear scar hardness before test on the GCI specimens are presented in Fig. 4 based on total number of measurement (frequency), 426. The GCI has very wide range of hardness ranging from the lowest value 185 HV to highest value 250 HV, a range of 65 HV.



Most of the hardness values are congregated in hardness range 205 HV~214 HV (79 measurements) and 210 HV ~ 214 HV (78 measurements). Based on the hardness test results, nine specimens were selected for friction and wear tests and grouped into three classes to represent low, medium and high hardness (Table 2) across the typical hardness range of GCI.

The distribution of GCI hardness value was as expected in which the high hardness range was found on previous literature <sup>11</sup> and as published in the standard (BS EN1561:2011). The wider hardness range from this work is similar to the GCI / ASTM 35B which is about 60 HB (60 HV) <sup>11</sup>. Hardness is one of the GCI properties that is influenced by many factors. It depends on aspects such as elements composition, size of flake graphite and distribution on the metal matrix and processing variable such as the casting cooling rate <sup>16, 28</sup>. Material that experiences a slow cooling rate produces lower hardness than rapidly cooled material. For example, different position in the same specimen in a casting bar (centre and corner position) produced different hardness (about 30 HB (30 HV)) due to the different cooling rate <sup>16</sup>. In addition, the cooling rate affects the microstructure of GCI by influencing the flake graphite size. A low cooling rate promoted bigger graphite size and produced lower hardness <sup>17</sup>.

## **Friction Analysis**

The COF for soybean oil lubricated GCI specimens with three different group of hardness (low, medium and high) are plotted in Fig. 5a. The unlubricated GCI specimens (low hardness) were also tested for comparison. This specimen started with high COF (0.292) which slowly reduced in magnitude. In contrast, for lubricated specimens, there was a low COF (about 0.09) at the beginning (running-in period), then it increased gradually and finally reached a

steady state condition after about 45 minutes. Significant COF differences are observed for unlubricated and lubricated specimens for low hardness compared to others. However, the differences of COF for lubricated specimens at medium and high hardness are not clearly observed so to show this difference in detail, Fig. 5(b) was plotted using the COF at 60 min. The COF for lubricated specimens is lowest at high hardness (0.122) compared to low hardness (COF = 0.140) about 13% difference. Soybean oil lubricant was found to improve the friction about 24% between lubricated (COF = 0.140) and unlubricated (COF = 0.185) specimens at low hardness. The ANOVA analysis of COF for all four above conditions (low, medium, high hardness and unlubricated specimens) were found to be significantly different ( $P < 0.05$ , Table 3). However, for medium and high hardness specimens, the COFs were not significantly different ( $P > 0.05$ , Table 4).

The COF profiles from this work are similar to those categorised by Blau<sup>29</sup>. The running-in behaviour for COF profile of unlubricated specimen could be best explained by the reorientation process of random crystal texture on the contact surface<sup>29</sup>. During the initial sliding process, the rearrangement of random atoms in the crystalline solids (lattice structure) occurred at near-surface area. The preferred texture is gradually achieved which is a steady state of microstructure resistance to sliding. The sliding resistance at this condition is less than the initial unworn surface of random orientation. A detailed discussion about this process has been previously elaborated on by Rigney and Hirth<sup>30</sup>.

The COF profile for unlubricated GCI in this study is similar with unlubricated GCI specimens tested at high speed (0.8 m/s) by Sugishita in which partial detachment of graphite was found at the start<sup>3</sup>. In the case of flake graphite cast iron, it takes some time for the graphite

to be near-uniformly distributed across the surface in order to reach a steady state value of friction coefficient which is lower than the initial value <sup>31</sup>.

It is possible that the running-in behaviour of lubricated specimens is due to the removal of lubricious contaminants from the contact surface <sup>32</sup> and disruption of surface oxide layer by increasing the metallic contact <sup>33</sup>. The removal of the graphite film due to supplement of lubricant was also reported by Sugishita <sup>3</sup>. Therefore, the response of COF for different material hardness is subject to the breakdown of oxide films near contact surface <sup>34</sup>. The high hardness specimens deform less therefore it is possible in preventing the breakdown of the oxide film. Thus, the lower friction is produced as showed by COF of high hardness specimens. In addition to this, the friction force is defined here as the summation of adhesive force and ploughing force as expressed by Bowden and Tabor <sup>8</sup>. The low hardness specimen is prone to deeper indentation by the steel ball thus, producing a wider track width and more deformation. The wider track width promotes a higher ploughing force to displace material, which accumulates in front of the slider (pin), and this increases the ploughing component of friction <sup>8</sup>. Furthermore, based on the Bowden and Tabor's formula, it can be shown that the plastic flow (close to the indentation hardness) may influence the adhesive component of friction in which low substrate hardness will produce a high friction coefficient.

## **Wear Analysis**

Fig. 6 shows the mass loss of GCI specimens after testing both with the contact lubricated with soybean oil and also dry (i.e. unlubricated), for the three different hardness groups. At low hardness, soybean oil slightly reduced the wear by 7% (50.38 mg of mass loss) compared to unlubricated specimens (54.38 mg). The wear was inversely proportional to the hardness. For

lubricated specimens, the mass loss is higher at low hardness (50.38 mg) compared to high hardness (12.90 mg), a difference of 74%. This shows that the difference in wear of lubricated specimens (between low and high hardness) is very significant and greatly influenced by the wide range of surface hardness of the GCI specimens.

From the calculation, the minimum film thickness,  $h_{\min}$  was  $1.08 \times 10^{-8}$  m and the lambda ratio,  $\lambda$  was 0.011. Based on this lambda value ( $\lambda = h_{\min} / \sigma^*$ ) which is less than 1, it is clearly shown that the minimum film thickness was much lower than the surface roughness. This means that the lubrication film was too thin to provide total surface separation. Thus, it is suggested that the lubrication regime is boundary <sup>27</sup>.

The main wear mechanisms for all of specimens are found to be abrasive in nature (Fig. 10). In abrasion, microcutting is the most efficient way to remove material <sup>35</sup> and penetrates into the specimen surface. This depends on the hardness of surface where a softer surface has lower penetration resistance. This depends on the hardness of surface where a softer surface has lower penetration resistance.

Based on ANOVA analysis, no significant difference in wear was found between low hardness specimens of lubricated and unlubricated, and also between medium and high hardness specimens with lubrication ( $P > 0.05$ , Table 5). However, the mass loss for all three specimens (low, medium and high hardness) are significantly different ( $P < 0.05$ , Table 6).

### **Wear Scar Appearance**

Fig. 7a shows the wear scar appearance after 60 minutes and they all have very similar formation, wavy-shaped scar indicating plastic deformation during sliding. The high hardness specimens produced the smallest wear scars.

The wavy-shaped wear scars in this study are similar to those seen in the work carried out by Plint involving a hard ball on soft plate<sup>36</sup>. The phenomenon of the wave-shaped scars could be explained by plastic ratchetting and shakedown limit. Ponter<sup>37</sup> reported the relation between Hertzian pressure- shear strength ratio and the COF (Fig. 8). At COF = 0.1 and Hertzian pressure- shear strength ratio more than 6 (values taken from this study), Ponter<sup>37</sup> suggests that the material deformation will enter the plastic ratcheting region. Plastic ratchetting occurs when the applied load exceeds the plastic shakedown limit<sup>38</sup>, in which the progressive plastic deformation of surfaces occurs during repeated sliding. In the ratchetting process, the large plastic strains are slowly accumulated and superposed during each sliding cycle. This accumulated plastic strain could translate into accumulated deformed material.

The images for specimens sectioned along the wear scar with low and high hardness are shown in Fig. 9. It is clearly seen that the graphite in GCI specimen is distributed heterogeneously with significant differences in form and distribution type. The graphite form for the high hardness specimen is similar to Form I with distribution C in BS EN ISO 945<sup>39</sup> with a lamellar shape. However, for low hardness specimens the graphite form is found to be closed to spheroidal shape (Form III, distribution D) which suggests undercooling of graphite occurred<sup>39</sup>. The constituents of graphite with a pearlite and ferrite matrix microstructure from this work are found to be similar with the GCI microstructure reported by Prasad in pin on disc sliding test<sup>40</sup>. Further investigation near to contact surface (etched surface) revealed that a very high amount of ferrite matrix is found in the low hardness specimen while in the high hardness specimen, a pearlite matrix is found everywhere. This ferrite matrix has a lower hardness than the pearlite which contributed to a lower strength. Furthermore, cracks and higher distortion of the pearlite

matrix seen near to the worn surface for the low hardness specimen suggests that higher plastic flow occurred during the sliding process.

### **Surface Waviness Analysis**

To further investigate the influence of hardness on the formation of wave-shaped scars, measurements resulting in the primary profile and the waviness profile of the specimens were taken along the sliding direction in the middle of the scars. A typical primary profile result shown in Fig. 7b depicts that the medium and high hardness specimens have shallow depth compared to the low hardness specimen. The specimen with high hardness produced the lowest surface waviness ( $W_a=15.00 \mu\text{m}$ ) while the low hardness specimen generated the highest surface waviness ( $W_a=37.82 \mu\text{m}$ ). However the unlubricated specimen (low hardness) is found to have lower surface waviness ( $W_a= 24.26 \mu\text{m}$ ) than the lubricated counterpart.

As material with high hardness has higher yield strength and more resistance to plastic strain, the measurements of waviness profile after test match this relationship. In the context of the wavy-shaped scar, the harder the specimen the lesser the surface waviness formed in the wear scar. This is due to lower plastic strain accumulated for harder specimens during plastic ratchetting process. Although the wear of the unlubricated specimen (low hardness) is higher than the lubricated counterpart (low hardness), in terms of waviness it shows a lower value compared to the lubricated specimen. The lower waviness value suggests that less plastic deformation occurred.

The removal of the graphite film of GCI due to addition of lubricant was reported by Sugishita<sup>3</sup>. The result from elemental analysis (Fig. 12) shows that more oxide layer (weight% of oxygen) is retained on the unlubricated specimen suggesting that the soybean oil could disrupt the graphite film as solid lubricant in soybean oil lubricated specimens. The role of an oxide layer in reducing friction and wear rates was reported<sup>33</sup>. This oxide layer could act as a protective layer in decreasing the level of penetration from ball to flat specimens. Therefore, lesser plastic deformation may occur and the accumulation of plastic strain could be reduced.

### **Surface Morphology**

The images of the wear scar of GCI specimen after testing (Fig. 10) were taken using the optical microscope at the different points (front, back and middle) shown in Fig. 11a. The surface roughness also were measured similarly (Fig. 11b). Generally, for the lubricated specimens (for all hardness), the wear mechanisms involved are similar.

The main wear mechanism is abrasive wear with some evidence of plastic flow of material on the surface leading to cracks and spalling. However, as the specimen hardness increased, the abrasive wear is seen to be reduced. This is shown by smoother surfaces on the front and back surfaces of high hardness specimens. A combination of abrasive and adhesive wear was found on the unlubricated specimens. The dark region on the unlubricated surfaces indicated that adhesive wear was taking place. Severe abrasive wear was also observed to occur in the middle point of wear scar.

It has been reported that the material hardness and abrasive wear resistance are proportional<sup>6</sup>. Therefore, a GCI specimen with lower hardness is less resistive to abrasive wear

and more likely to create abrasion marks on the surface. Measurements of surface roughness after test (Fig. 11b) have confirmed the relation between hardness and surface roughness as reported that surfaces roughness decreases when hardness increases <sup>4</sup>.

## **Elemental Analysis**

The surface morphology of specimens was inspected under SEM to further investigate the wear mechanism in smaller area with higher magnification (1000x). EDX analysis also was used in order to analyse the elements on the surface. Generally, from the SEM images (Fig. 12) the wear mechanisms found in all specimens are abrasive and surface fatigue, confirming the earlier observations. For lower specimen hardness (lubricated and unlubricated), some delamination, cracks and pitting were also observed.

In EDX analysis, the oxygen was compared on each specimen surface in investigating the oxide layer on the surface. For lubricated specimens, a high amount of oxygen was detected on high hardness specimens compared to low hardness specimens. However, the amount of oxygen is found highest on unlubricated specimens compared to others. It was reported that the metal oxide provides a protective layer during sliding <sup>41</sup>. In this study, the higher oxygen value that exists on high hardness specimens (lubricated) suggests that more oxide is retained on the surface compared to the low hardness specimens. This is due to less deformation occurring on the harder material thus preventing the oxide layer from breaking down. However, the lower amount of oxygen present on the lubricated specimen compared to unlubricated specimen suggests that the oxidation process of the lubricant (soybean oil) was take place during the sliding process. This seems particularly likely in this work as soybean oil is an unsaturated fatty



acid with doubled bonded carbon atoms in the molecular structure and is therefore more susceptible to oxidation at elevated temperatures <sup>42</sup>. It was also noticed that higher carbon content produced in the unlubricated specimen compared to the lubricated suggests that the graphite is retained on the surface of GCI during the sliding process.

## **Conclusions**

From the outcome of the experiments above, the following conclusion can be highlighted:

- The use of bulk hardness to represent GCI specimen hardness should be avoided. This bulk hardness would misrepresent the friction and wear data as hardness differs very much in GCI specimens.
- The difference in specimen hardness of GCI revealed a great influence on the wear and friction test data. The inconsistent wear and friction results may be produced for repeated tests if the hardness characterisation of GCI specimen has not been performed properly.
- A hardness characterisation of GCI specimens closed to the wear scar region prior to a test is very important in producing robust results of wear and friction. A high hardness of material should be selected in producing lower friction and high wear resistance.
- The wide hardness range that GCI has could contribute to the non-uniform wear and friction at contact interface for machine parts made from this material.
- The influence of soybean oil over wide range of GCI specimen hardness is significant. In terms of lubrication, the soybean oil showed less contribution to wear resistance (about 7%) but rather serves to decrease friction (about 24%) compared to an unlubricated surface.

## References

1. Taylor BJ, Eyre TS. A review of piston ring and cylinder liner materials. *Tribology International*. 1979; 12: 79-89.
2. Glaeser WA. *Materials for Tribology*. Amsterdam, Netherlands: Elsevier, 1992.
3. Sugishita J, Fujiyoshi S. The effect of cast iron graphites on friction and wear performance I: Graphite film formation on grey cast iron surfaces. *Wear*. 1981; 66: 209-21.
4. Bian S, Maj S, Borland DW. The unlubricated sliding wear of steels: The role of the hardness of the friction pair. *Wear*. 1993; 166: 1-5.
5. Khrushov MM. Principles of abrasive wear. *Wear*. 1974; 28: 69-88.
6. Moore MA. The relationship between the abrasive wear resistance, hardness and microstructure of ferritic materials. *Wear*. 1974; 28: 59-68.
7. Mokhtar MOA, Zaki M, Shawki GSA. Effect of mechanical properties on frictional behaviour of metals. *Tribology International*. 1979; 12: 265-8.
8. Bowden FP, Tabor D, Palmer F. The Friction and Lubrication of Solids. *American Journal of Physics*. 1951; 19: 428-9.
9. Mokhtar MOA. The effect of hardness on the frictional behaviour of metals. *Wear*. 1982; 78: 297-304.
10. BS EN 1561:2011. Founding Grey Cast Iron.
11. A.J. Shturmakov CRL, Jr. Predictive Analysis of Mechanical Properties in Commercial Gray Iron. *American Foundry Society*. 2002; 99: 609-15.
12. Terheci M, Manory RR, Hensler JH. The friction and wear of automotive grey cast iron under dry sliding conditions Part 1-relationships between wear loss and testing parameters. *Wear*. 1995; 180: 73-8.
13. Rac A. Influence of load and speed on wear characteristics of grey cast iron in dry sliding — selection for minimum wear. *Tribology International*. 1985; 18: 29-33.
14. Liu YC, Schissler JM, Mathia TG. The influence of surface oxidation on the wear resistance of cast iron. *Tribology International*. 1995; 28: 433-8.
15. Sugishita J, Fujiyoshi S. The effect of cast iron graphites on friction and wear performance. *Wear*. 1981; 68: 7-20.
16. Angus HT. *Cast iron: physical and engineering properties*. London: Butterworth, 2013.
17. Adedayo AV. Relationship between graphite flake sizes and the mechanical properties of grey iron. *International Journal of Materials Science and Applications*. 2013; 2: 94-8.
18. Masjuki HH, Maleque MA, Kubo A, Nonaka T. Palm oil and mineral oil based lubricants - their tribological and emission performance. *Tribology International*. 1999; 32: 305-14.
19. Imran A, Masjuki H, Kalam M, et al. Study of Friction and Wear Characteristic of Jatropa Oil Blended Lube Oil. *Procedia Engineering*. 2013; 68: 178-85.
20. Castro W, Perez JM, Erhan SZ, Caputo F. A study of the oxidation and wear properties of vegetable oils: Soybean oil without additives. *JAOCS, Journal of the American Oil Chemists' Society*. 2006; 83: 47-52.
21. Adhvaryu A, Erhan SZ. Epoxidized soybean oil as a potential source of high-temperature lubricants. *Industrial Crops and Products*. 2002; 15: 247-54.

22. Dodos GS, Anastopoulos G, Zannikos F. Tribological evaluation of biobased lubricant basestocks from cottonseed and soybean oils. *SAE International Journal of Fuels and Lubricants*. 2010; 3: 378-85.
23. Bartz WJ. Lubricants and the environment. *Tribology International*. 1998; 31: 35-47.
24. Wilson B. Lubricants and functional fluids from renewable sources. *Industrial Lubrication and Tribology*. 1998; 50: 6-15.
25. Hollinghurst R. High Temperature Lubrication Requirements of European Gasoline and Diesel Engines for Cars. *SAE International*. 1974; 740973: 3057-76.
26. Bernard JH. *Fundamentals of fluid film lubrication*. New York: Marcel Dekker, 2004.
27. Ian MH. *Tribology : friction and wear of engineering materials*. London: Butterworth-Heinemann, 1992.
28. Brown JR. *Foseco Foundryman's Handbook*. Oxford: Butterworth-Heinemann, 2000.
29. Blau PJ. Interpretations of the friction and wear break-in behavior of metals in sliding contact. *Wear*. 1981; 71: 29-43.
30. Rigney DA, Hirth JP. Plastic deformation and sliding friction of metals. *Wear*. 1979; 53: 345-70.
31. Buckley DH. Effect of carbon content on friction and wear of cast irons. *NASA Technical Paper*. 1977; 1052.
32. Blau PJ. *Friction science and technology: from concepts to applications*. Boca Raton: CRC press, 2008.
33. Rabinowicz E. Lubrication of metal surfaces by oxide films. *ASLE TRANSACTIONS*. 1967; 10: 400-7.
34. Moore AJW, Tegart WJM. Relation between Friction and Hardness. *Proceedings of the Royal Society of London Series A, Mathematical and Physical Sciences*. 1952; 212: 452-8.
35. Rigney DA. The roles of hardness in the sliding behavior of materials. *Wear*. 1994; 175: 63-9.
36. Plint G. The Sliding Hertzian Point Contact in Tribotesting: Understanding its Limitations as a Model of Real Systems. In: *STLE 70th Annual Meeting & Exhibition, 17 May -21 May 2015*. Texas: STLE.
37. Ponter ARS, Hearle AD, Johnson KL. Application of the kinematical shakedown theorem to rolling and sliding point contacts. *Journal of the Mechanics and Physics of Solids*. 1985; 33: 339-62.
38. Williams JA. The influence of repeated loading, residual stresses and shakedown on the behaviour of tribological contacts. *Tribology International*. 2005; 38: 786-97.
39. BS EN ISO 945-1: 2008. *Microstructure of cast irons Part 1: Graphite classification by visual analysis*.
40. Prasad BK. Sliding wear response of a cast iron under varying test environments and traversal speed and pressure conditions. *Wear*. 2006; 260: 1333-41.
41. Stott FH, Wood GC. The influence of oxides on the friction and wear of alloys. *Tribology International*. 1978; 11: 211-8.
42. Lou A.T.Honary, Ritcher E. *Biobased lubricants and greases: Technology and Products*. Chichester: John Wiley and Sons, 2011.

## Tables

**Table 1.** Physical properties of soybean oil

Dynamic viscosity at 40°C	30.72 cP
Dynamic viscosity at 100°C	7.10 cP
Density at 40°C	0.9082 g/ml
Density at 100°C	0.8674 g/ml
Total Acid Number	0.98 mgKOH/g

**Table 2.** Hardness of selected nine flat specimens grouped into low, medium and high hardness

Specimen number	Wear Scar Hardness (HV)	Average Hardness (HV)	Hardness group
1	207.7		
2	206.7	206.5	low
3	205.0		
4	224.3		
5	224.3	223.4	medium
6	221.7		
7	240.0		
8	248.7	245.5	high
9	247.7		

**Table 3.** ANOVA analysis of COF for low, medium and high hardness specimens with unlubricated specimens

<i>Groups</i>	<i>Count</i>	<i>Sum</i>	<i>Average</i>	<i>Variance</i>
Low	3	0.421	0.140	3.81E-05
Medium	3	0.370	0.123	6.35E-05
High	3	0.365	0.122	2.19E-05
Unlubricated	3	0.557	0.185	2.62E-05

ANOVA						
<i>Source of Variation</i>	<i>SS</i>	<i>df</i>	<i>MS</i>	<i>F</i>	<i>P-value</i>	<i>F crit</i>
Between Groups	0.007983	3	0.002661	71.1270	4.14E-06	4.0661
Within Groups	0.000299	8	3.74E-05			
Total	0.008283	11				

**Table 4.** ANOVA analysis of COF for medium and high hardness specimens

<i>Groups</i>	<i>Count</i>	<i>Sum</i>	<i>Average</i>	<i>Variance</i>
Medium	3	0.370179	0.123	6.35E-05
High	3	0.364988	0.122	2.19E-05

ANOVA						
<i>Source of Variation</i>	<i>SS</i>	<i>df</i>	<i>MS</i>	<i>F</i>	<i>P-value</i>	<i>F crit</i>
Between Groups	4.49E-06	1	4.49E-06	0.1052	0.7618	7.7086
Within Groups	0.000171	4	4.27E-05			
Total	0.000175	5				

**Table 5.** ANOVA analysis of mass loss for low and unlubricated specimens

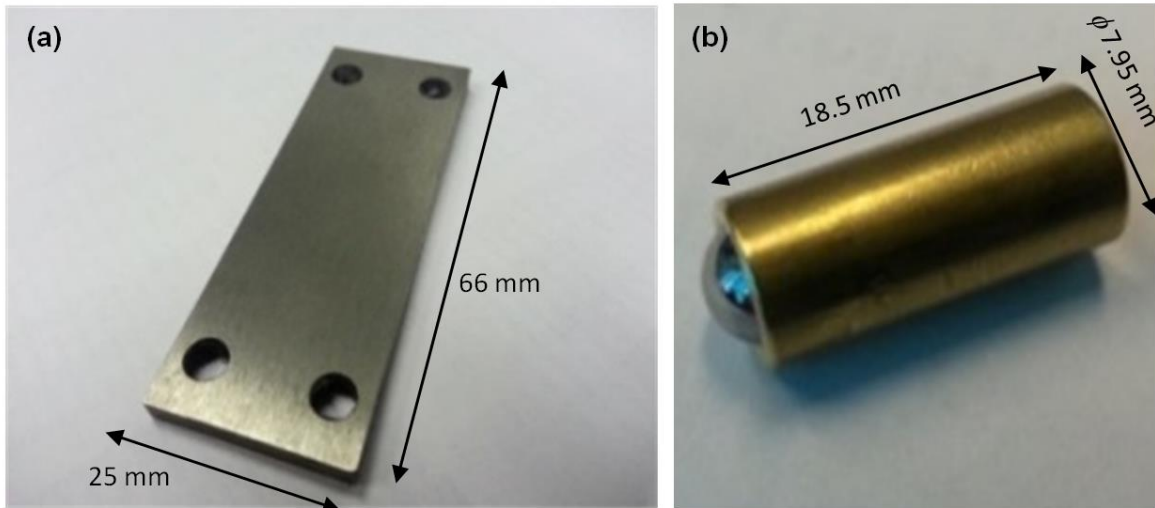
<i>Groups</i>	<i>Count</i>	<i>Sum</i>	<i>Average</i>	<i>Variance</i>		
Low	3	151.14	50.38	9.51		
Unlubricated	3	163.13	54.38	33.91		
<b>ANOVA</b>						
<i>Source of Variation</i>	<i>SS</i>	<i>df</i>	<i>MS</i>	<i>F</i>	<i>P-value</i>	<i>F crit</i>
Between Groups	23.96	1	23.96	1.1037	0.3527	7.7086
Within Groups	86.83	4	21.71			
Total	110.79	5				

**Table 6.** ANOVA analysis of mass loss for low, medium and high hardness specimens

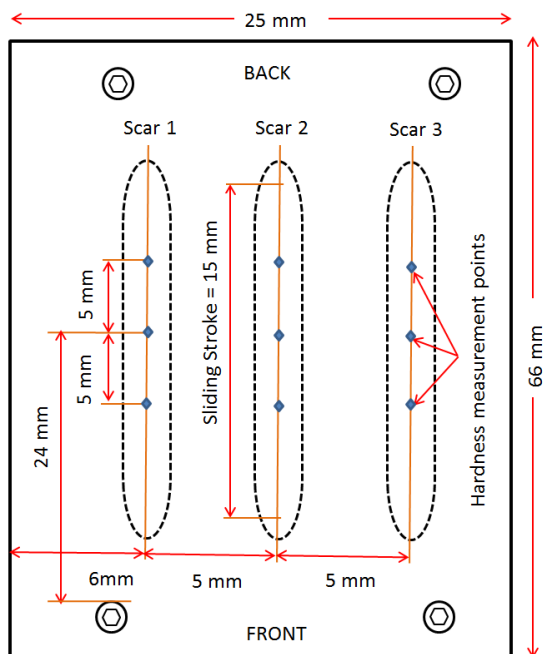
<i>Groups</i>	<i>Count</i>	<i>Sum</i>	<i>Average</i>	<i>Variance</i>		
Low	3	151.14	50.38	9.5101		
Med	3	58.41	19.47	39.2896		
High	3	38.71	12.90333	2.172933		
<b>ANOVA</b>						
<i>Source of Variation</i>	<i>SS</i>	<i>df</i>	<i>MS</i>	<i>F</i>	<i>P-value</i>	<i>F crit</i>
Between Groups	2403.05	2	1201.525	70.7158	6.74E-05	5.1432
Within Groups	101.9453	6	16.99088			
Total	2504.995	8				

## List of Figures

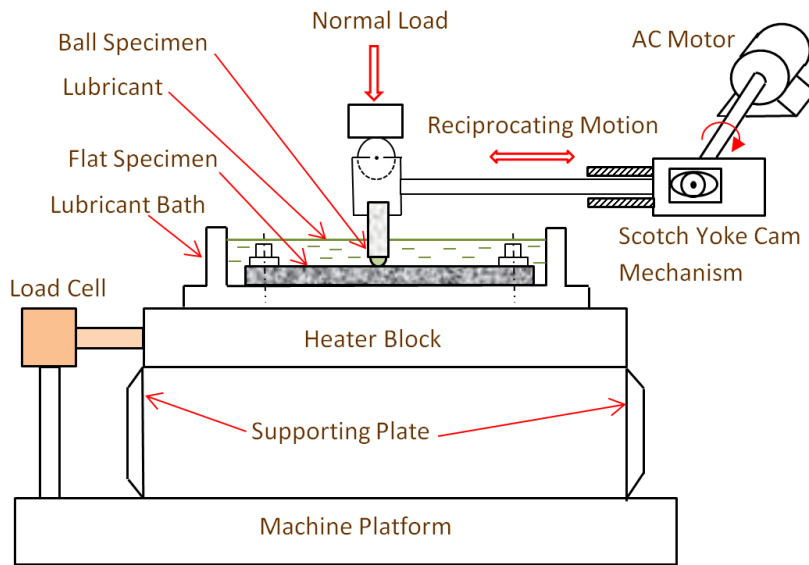
**Figure 1.** Geometry of (a) flat and (b) ball specimens



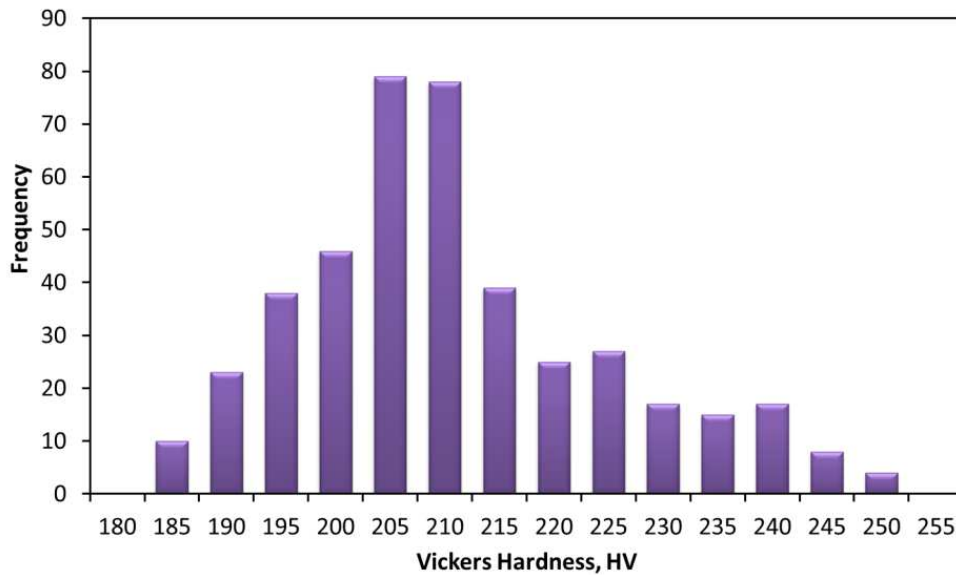
**Figure 2.** Hardness measurement at three points on each targeted wear scar (dotted line: Scar 1, Scar 2 and Scar 3) of specimen before test



**Figure 3.** Schematic of ball on flat reciprocating sliding contact with lubricant oil

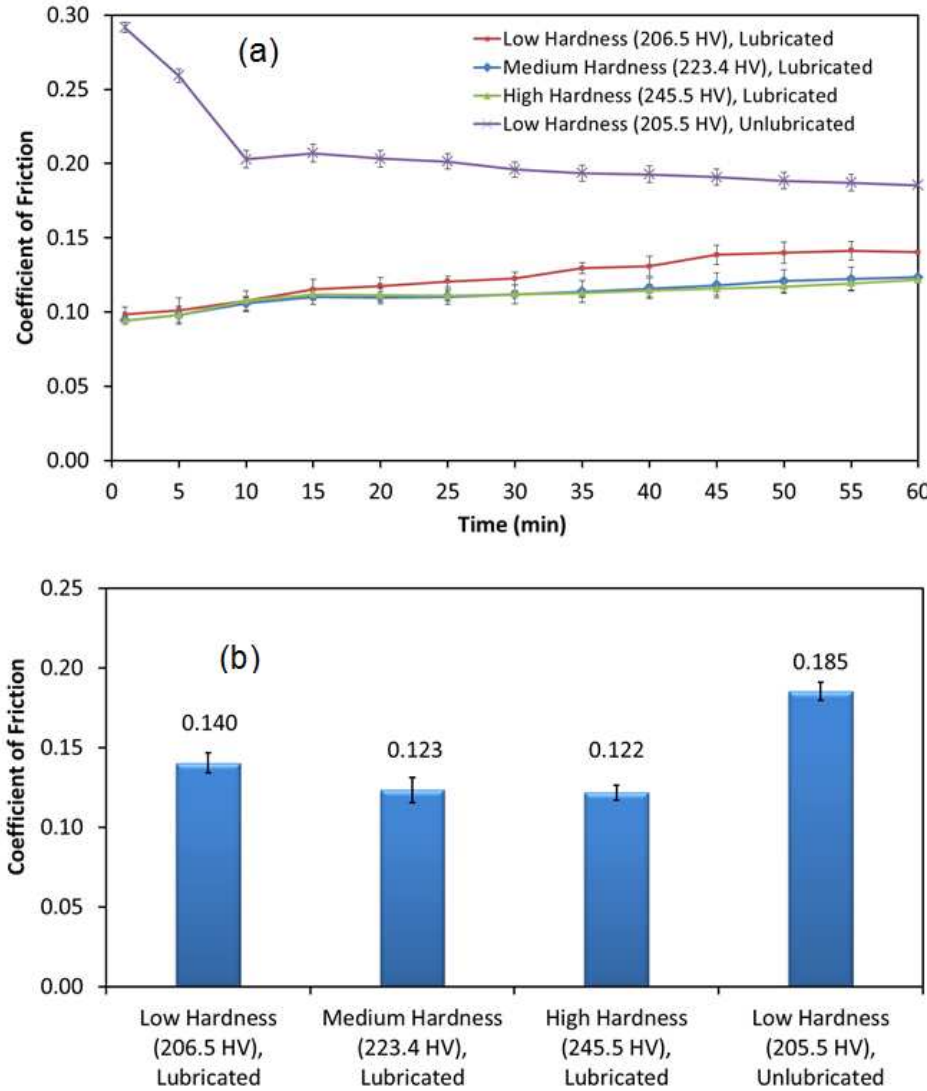


**Figure 4.** Distribution of GCI specimen hardness measured on intended wear scar areas before testing. The frequency denotes the number of hardness measurements performed (total measurement = 426).

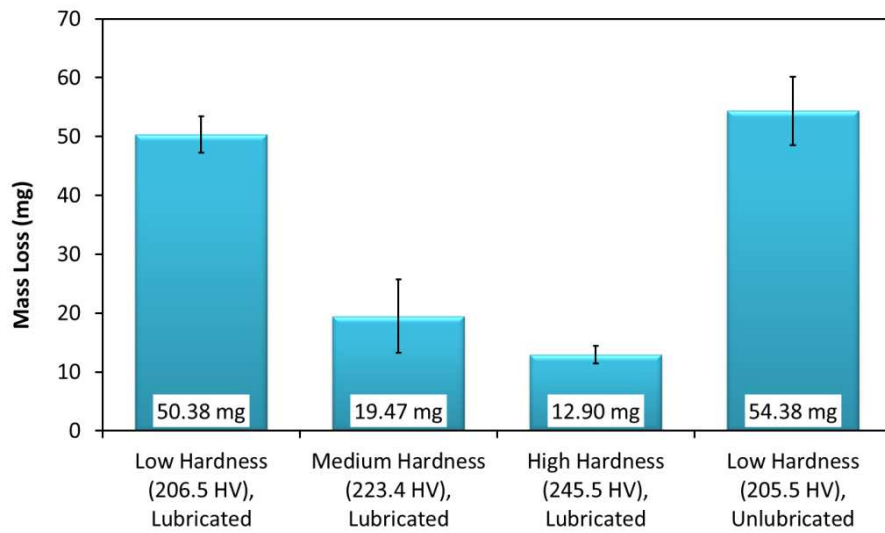




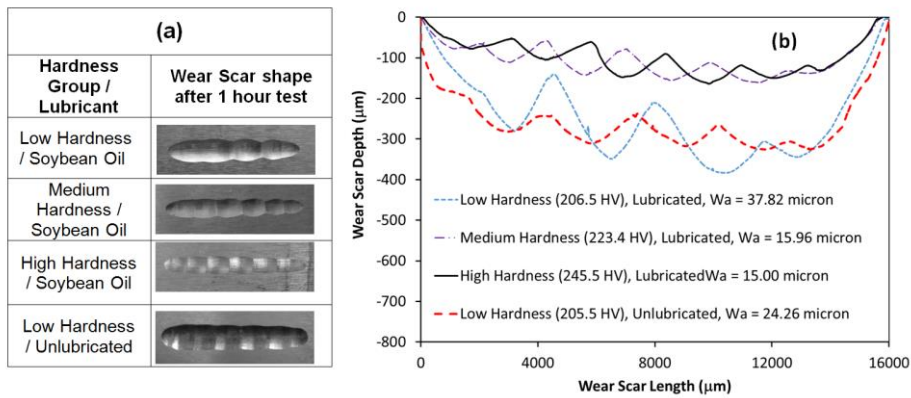
**Figure 5.** (a) Coefficient of Friction versus time and (b) Coefficient of Friction value at 60 minutes of specimens with low, medium and high hardness



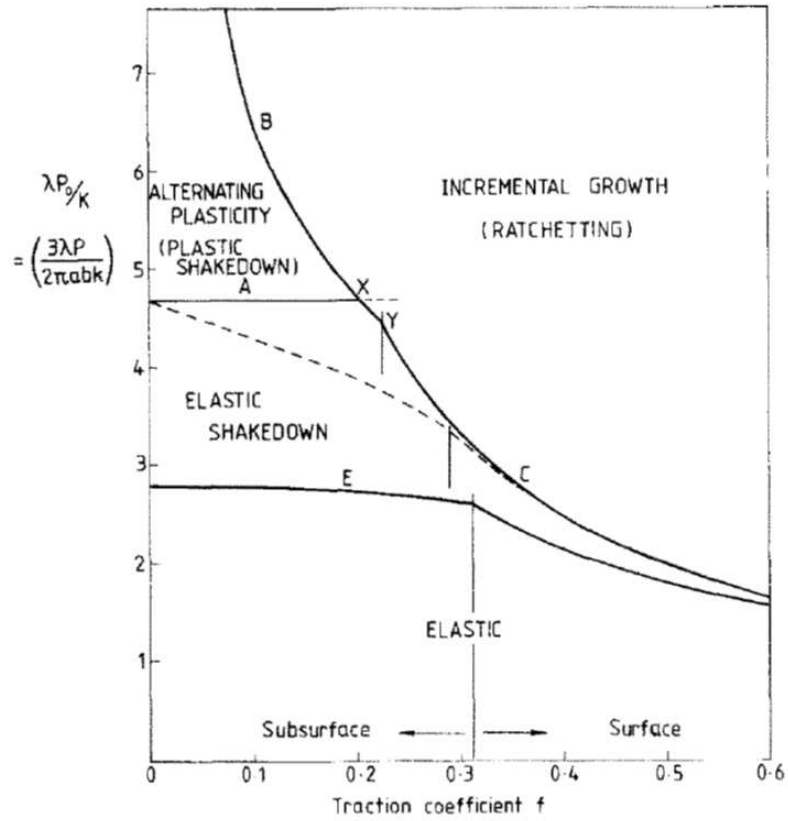
**Figure 6.** Mass Loss of specimens with low, medium and high hardness




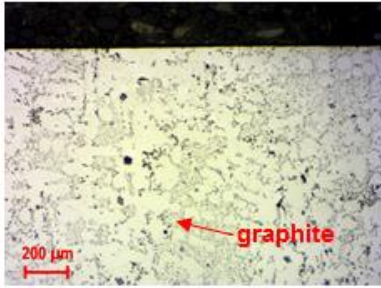
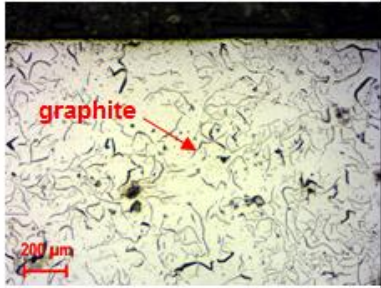
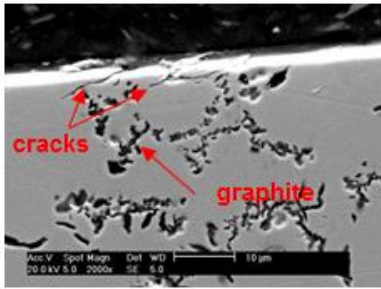
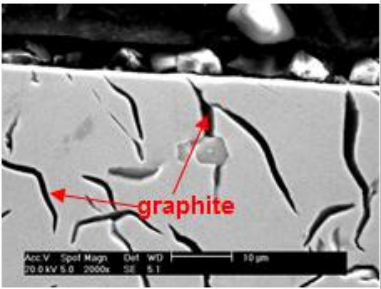
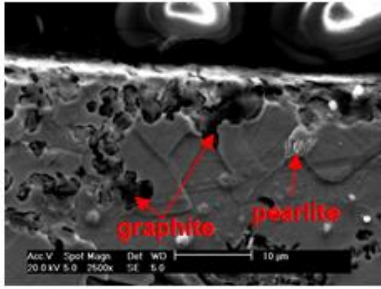
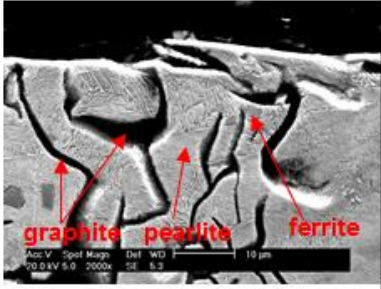
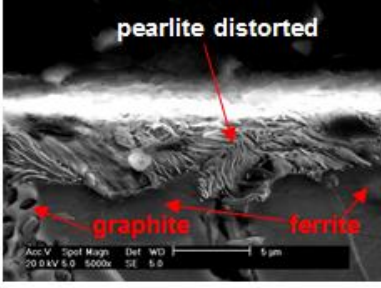
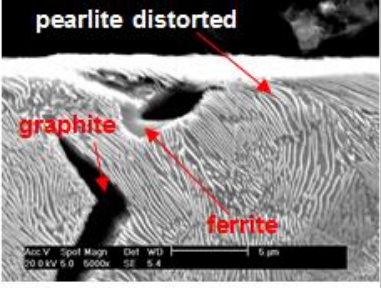
**Figure 7.** (a) Wear scar appearance and (b) Primary profile of specimens with low, medium and high hardness



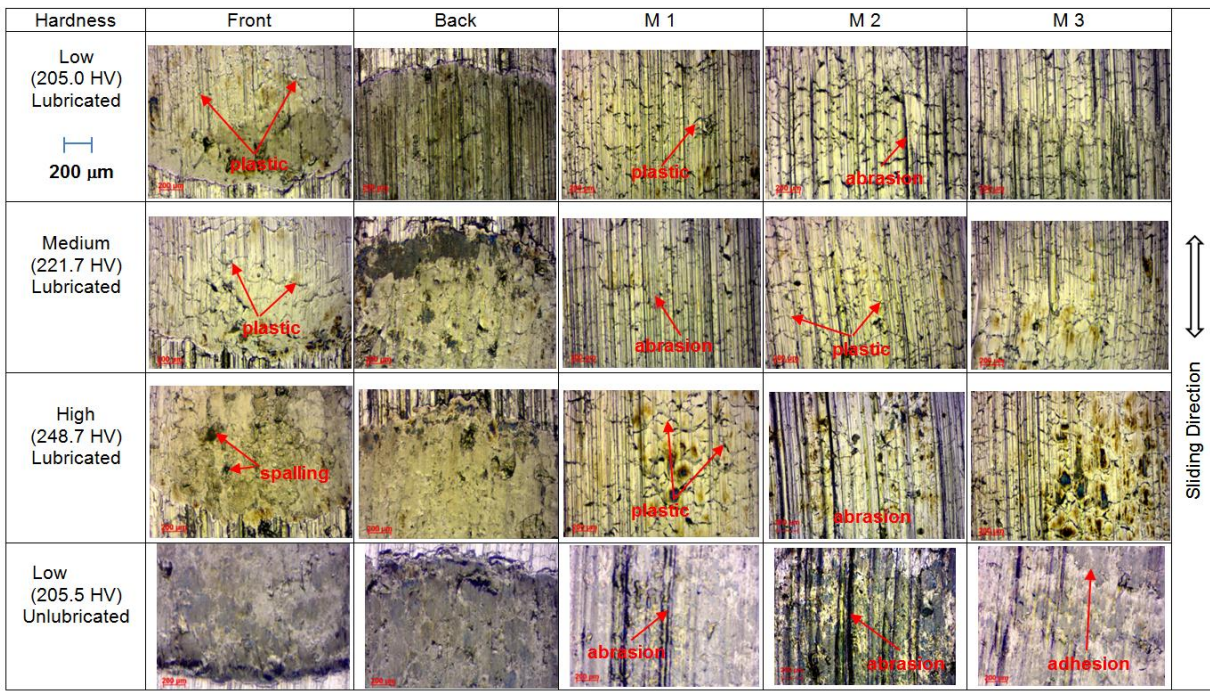
**Figure 8.** The elastic, elastic shakedown, plastic shakedown and ratchetting region associated with Hertzian pressure,  $P_0$  -shear strength ratio,  $K$  on coefficient of friction,  $f$  for sliding point contact <sup>37</sup>



**Figure 9.** Sectioning images of wear scar for low and high hardness specimens

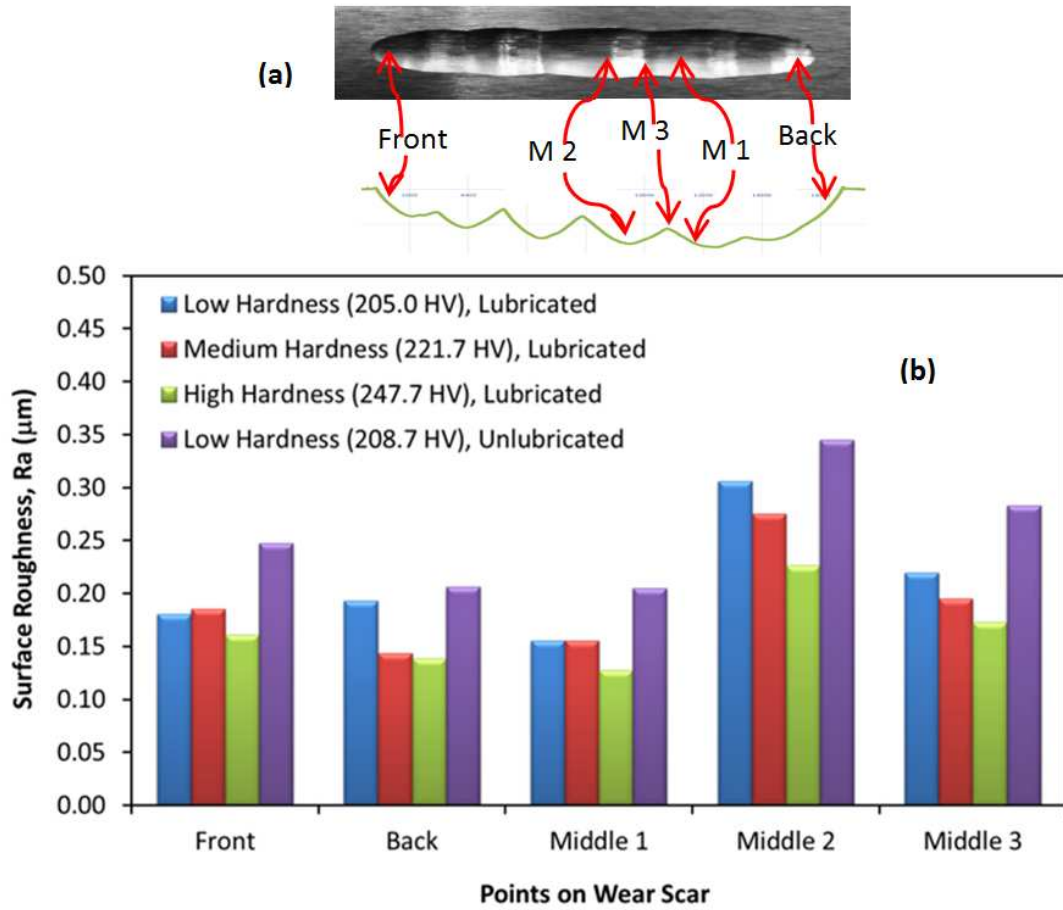
	Low Hardness Specimen	High Hardness Specimen
	 Sliding Direction	
Before Etching (Optical Microscope)		
Before Etching (SEM)		
After Etching (SEM)		
		

**Figure 10.** Wear scar images under optimal microscope taken at different point (Figure 11a)



**Figure 11.** (a) Points on Wear Scar where the images and roughness are measured and (b)

Surface roughness across wear scar taken at different points based on Figure 11a



**Figure 12.** Surface morphology under SEM (1000X) and elemental analysis

Hardness	Wear Scar Image	Wear Mechanism	Element Analysis		
			Element	Weight %	Atomic %
Low (205.0 HV) Lubricated		abrasion	<b>C</b>	3.77	14.56
		surface fatigue	<b>O</b>	1.43	4.15
		pitting	<b>Si</b>	2.91	4.80
		delamination	<b>P</b>	0.15	0.22
			<b>S</b>	0.00	0.00
			<b>Mn</b>	0.84	0.55
			<b>Fe</b>	90.91	75.56
Medium (221.7 HV) Lubricated		abrasion	<b>C</b>	3.27	12.53
		surface fatigue	<b>O</b>	2.44	7.03
			<b>Si</b>	3.30	5.41
			<b>P</b>	0.05	0.07
			<b>S</b>	0.01	0.01
			<b>Mn</b>	0.67	0.56
			<b>Fe</b>	90.26	74.38
High (248.7 HV) Lubricated		abrasion	<b>C</b>	3.88	14.63
		surface fatigue	<b>O</b>	2.49	7.03
			<b>Si</b>	3.00	4.84
			<b>P</b>	0.00	0.00
			<b>S</b>	0.04	0.05
			<b>Mn</b>	0.69	0.57
			<b>Fe</b>	89.90	72.88
Low (205.5 HV) Unlubricated		abrasion	<b>C</b>	7.13	23.33
		surface fatigue	<b>O</b>	5.27	12.95
		delamination	<b>Si</b>	2.84	3.97
		cracks	<b>P</b>	0.05	0.07
			<b>S</b>	0.05	0.06
			<b>Mn</b>	0.55	0.40
			<b>Fe</b>	84.12	59.23